Effects of cyclic four-spin exchange on the magnetic properties of the CuO2 plane

doi: 10.1103/PhysRevB.47.11329

Effects of cyclic four-spin exchange on the magnetic properties of the CuO_2 plane

Y. Honda, Y. Kuramoto, and T. Watanabe
Department of Applied Physics, Tohoku University, Sendai 980, Japan
(Received 6 May 1992)

For the CuO_2 square lattice, as a parent system of high-T_c superconductors, a numerical study has suggested that the effective-spin model contains a large cyclic four-spin exchange interaction J_c. This paper investigates the effects of J_c upon magnetic Raman scattering and upon properties of the ground state by an exact numerical method mainly for a 16-site cluster. It is found that the main Raman peak with the B_{1g} symmetry is shifted by 20% to the lower-energy side with a realistic magnitude for J_c, which is about one fourth the size of the nearest-neighbor exchange J. Accordingly a value of J extracted from analyses of experimental data becomes larger by 10% than that estimated with the use of the Heisenberg model. Furthermore the four-spin exchange enhances a shoulder due to multimagnon states at an energy of about $4J$, and this result compares favorably with the experimental line shape. Detailed discussion is given on the effect of the four-spin exchange upon the ground-state properties such as the staggered magnetization, the ground-state energy, weight of various spin configurations, and the spin-spin correlation function.

I. INTRODUCTION

In some copper oxides such as La_2CuO_4, which is known as a parent insulator of the high-T_c superconducting systems, electronic states of the CuO_2 plane are frequently described in terms of the two-dimensional spin-1/2 Heisenberg model. For these materials the Raman-scattering spectrum with the B_{1g} symmetry has a main feature associated with the two-magnon bound state. A large antiferromagnetic exchange interaction J between nearest-neighbor copper sites has been deduced from analysis of Raman-scattering experiments.[1–6] For example, about 1000 cm^{-1} is estimated as the value of J for La_2CuO_4. This value is roughly consistent with that obtained from inelastic neutron scattering[7–10] and is larger than that of other magnetic materials.[6,11]

In contrast to spin-1 magnetic materials,[11] where the conventional spin-wave theory without taking account of the magnon-magnon interactions[12,13] explains the spectral line shape reasonably well, the spectra of the high-T_c oxides have the following distinctive features. First, the linewidth of the two-magnon peak[1–6] is much broader than the prediction of the spin-wave theory. Secondly, the intensity of the spectra extends up to 8000 cm^{-1},[5,6] which is well beyond the cutoff energy at $4J$ predicted by the spin-wave theory.[12,13] Thirdly, at low temperatures a shoulder has been found at the high-energy side ($\sim$ 4500 cm^{-1}) of the two-magnon peak in the B_{1g} spectra.[6] It is interesting that La_2NiO_4, which is isostructural with La_2CuO_4 but has spin 1, does not have this feature.

On the theoretical side it has been found by an expansion from the Ising limit[14] that the large quantum spin fluctuations in the ground state are intrinsic to the two-dimensional spin-1/2 Heisenberg model. The spectral moments deduced by the theory is consistent with the broad linewidth of the B_{1g} spectra.[14,15] However, by the nature of the theory it is not possible to derive the spectrum itself. On the other hand, with the use of the exact diagonalization method for small clusters,[16,17] the Raman spectrum has been computed for the Heisenberg model and the t-J model.

Apart from the analysis of the magnetic Raman scattering with use of the Heisenberg and t-J models, search for a more accurate effective model for the CuO_2 plane has been made.[18,19] A motivation of the present study is a theoretical report,[19] which has proposed the existence of a large cyclic four-spin exchange interaction J_c in the CuO_2 plane. J_c has been estimated as about one-fourth of the nearest-neighbor exchange interaction J. It is natural to expect that this large four-spin exchange influences the magnetic property of the CuO_2 plane in various aspects. Thus in this study we investigate the effect of the four-spin exchange upon the magnetic Raman scattering. Of particular interest is whether the high-energy shoulder appearing in the Raman spectrum at low temperatures is related to the cyclic four-spin exchange. We also estimate the Heisenberg exchange J from analysis of experimental results with account of J_c. A preliminary report on the theory of the Raman spectrum has been published.[20]

In addition, we study the effect of the four-spin exchange on the ground-state properties of the system such as the ground-state energy, staggered magnetization, weights of various spin configurations, contributions of each interaction to the total energy, and spin-spin correlation functions. Though J_c has been estimated to be about one fourth of J in the actual CuO_2 plane, we vary J_c up to $1.5J$ in order to see more clearly some consequences of the four-spin exchange.

We use the exact diagonalization method mainly for a 4×4 square lattice and restrict ourselves to the insulating phase of the CuO_2 plane.

II. SPIN HAMILTONIAN AND RAMAN INTERACTION

In the CuO_2 plane the large Coulomb repulsion ($U \sim 8-10$ eV) prevents two holes from doubly occupying a

copper site. Then the insulating phase of the system is usually described with one use of the two-dimensional spin-1/2 Heisenberg model. However, in copper oxide the energy difference between hole levels at copper and oxygen sites is not much larger than the hybridization energy between $3d$ and $2p$ orbitals. This causes some higher-order effects of hybridization significant. For example, in addition to the Heisenberg exchange between nearest-neighbor spins, cyclic four-spin permutations are likely to occur in the CuO_2 plane. The cyclic spin exchange has been known in other materials such as solid ^{3}He.[21] Thus we work with the following effective Hamiltonian

$$\begin{aligned}\mathcal{H} &= \mathcal{H}_H + \mathcal{H}_{4s}, \\ \mathcal{H}_H &= J\sum_{\langle i,j\rangle}\mathbf{S}_i\cdot\mathbf{S}_j - \frac{J}{4}\sum_{\langle i,j\rangle} n_i n_j \ , \\ \mathcal{H}_{4s} &= J_c \sum_{\langle i,j,k,l\rangle}\{(\mathbf{S}_i\cdot\mathbf{S}_j)(\mathbf{S}_k\cdot\mathbf{S}_l)+(\mathbf{S}_i\cdot\mathbf{S}_l)(\mathbf{S}_j\cdot\mathbf{S}_k) \\ &\quad -(\mathbf{S}_i\cdot\mathbf{S}_k)(\mathbf{S}_j\cdot\mathbf{S}_l)\} \qquad (1)\end{aligned}$$

where $\mathbf{S}_i$ denotes a spin-1/2 operator at site i of a two-dimensional square lattice. n_i is a number operator at site i. J and J_c represent the nearest-neighbor exchange interaction and a cyclic four-spin exchange interaction, respectively. $\mathcal{H}_H$ describes the isotropic spin-1/2 Heisenberg model. In this Hamiltonian the sum is over nearest-neighbor pairs of spins. In $\mathcal{H}_{4s}$, $\langle i,j,k,l\rangle$ means the sum over groups of four spins in a unit square. The meaning of $\mathcal{H}_{4s}$ may become clearer if it is rewritten in terms of cyclic four-spin permutation operator P_{ijkl} as

$$\begin{aligned}&(\mathbf{S}_i\cdot\mathbf{S}_j)(\mathbf{S}_k\cdot\mathbf{S}_l)+(\mathbf{S}_i\cdot\mathbf{S}_l)(\mathbf{S}_j\cdot\mathbf{S}_k)-(\mathbf{S}_i\cdot\mathbf{S}_k)(\mathbf{S}_j\cdot\mathbf{S}_l) \\ &\quad = \tfrac{1}{4}(P_{ijkl}+P_{ijkl}^{-1}) \\ &\quad\quad -\tfrac{1}{4}(\mathbf{S}_i\cdot\mathbf{S}_j+\mathbf{S}_j\cdot\mathbf{S}_k+\mathbf{S}_k\cdot\mathbf{S}_l+\mathbf{S}_l\cdot\mathbf{S}_i) \\ &\quad\quad -\tfrac{1}{4}(\mathbf{S}_i\cdot\mathbf{S}_k+\mathbf{S}_j\cdot\mathbf{S}_l)-\tfrac{1}{16}\ . \qquad (2)\end{aligned}$$

It has been found that J_c amounts to about one-fourth of J in a numerical study of CuO_2 plane.[19] We note that two-spin exchanges between nearest-neighbor and next-nearest-neighbor sites appear in Eq. (2). It has been shown[19] that the next-nearest-neighbor exchange not contained in the form of Eq. (2) is negligibly small in the CuO_2 plane.

The two-magnon Raman interaction,[22] which couples the light and the pairs of spins is given by

$$\mathcal{H}_R = C_R\sum_{\langle i,j\rangle}(\mathbf{E}_{\rm inc}\cdot\boldsymbol{\sigma}_{ij})(\mathbf{E}_{\rm sc}\cdot\boldsymbol{\sigma}_{ij})\mathbf{S}_i\cdot\mathbf{S}_j \qquad (3)$$

where $\mathbf{E}_{\rm inc}$ and $\mathbf{E}_{\rm sc}$ are unit vectors of the electric fields for incident and scattered light respectively. $\boldsymbol{\sigma}_{ij}$ is an unit vector between the nearest-neighbor i and j sites. We take unit magnitude for the coupling constant C_R. This Raman interaction flips nearest-neighbor spins and makes two magnons in the adjacent sites. These magnons interact strongly with each other because of their closeness. Hence, the spectrum given by this Raman interaction cannot be interpreted in terms of a simple picture of noninteracting magnons.

III. MAGNETIC RAMAN SCATTERING

A. Numerical method

We diagonalize the effective Hamiltonian $\mathcal{H}$ on the 4×4 square lattice with the periodic boundary condition in the subspace where the z component of total spin is zero. We use a modified Lanczos method.[23]

The Raman spectrum $I_0(\omega)$ at $T=0$ is given by

$$I_0(\omega) = \frac{1}{N}\sum_i |\langle\Psi_i|\mathcal{H}_R|\Psi_0\rangle|^2\delta(\omega-(E_i-E_0))\ , \qquad (4)$$

where $|\Psi_0\rangle$ is the ground state of $\mathcal{H}$ with energy E_0 and $|\Psi_i\rangle$ is the ith eigenstate with energy E_i. For numerical calculation it is convenient to introduce a related quantity $I(\omega)$ as follows:

$$I(\omega) = -\frac{1}{N\pi}\mathrm{Im}\left\langle\Psi_0\left|\mathcal{H}_R\frac{1}{\omega+E_0-\mathcal{H}+i\gamma}\mathcal{H}_R\right|\Psi_0\right\rangle\ , \qquad (5)$$

where γ gives a width to each excited state. In the limit of small γ one recovers $I_0(\omega)$ defined by Eq. (4).

Let us introduce a function $A(z)$ as follows:

$$A(z) \equiv \left\langle 0\left|\frac{1}{z-\mathcal{H}}\right|0\right\rangle\ , \qquad (6)$$

where $|0\rangle$ is defined by

$$|0\rangle \equiv \mathcal{H}_R|\Psi_0\rangle\ . \qquad (7)$$

Then the spectral intensity $I(\omega)$ is given by

$$I(\omega) = -\frac{1}{N\pi}\mathrm{Im}A(\omega+E_0+i\gamma)\ . \qquad (8)$$

We use a continued fraction method[24] and represent $A(z)$ as follows:

$$A(z) = \cfrac{\langle 0|0\rangle}{z-a_0-\cfrac{b_1}{z-a_1-\cfrac{b_2}{z-a_2-\cdots}}}\ , \qquad (9)$$

where the coefficients $\{a_n, b_n\}$ are derived through the following relations:

$$a_n \equiv \frac{\langle n|\mathcal{H}|n\rangle}{\langle n|n\rangle}\ , \qquad (10)$$

$$b_n \equiv \frac{\langle n-1|\mathcal{H}|n\rangle}{\langle n-1|n-1\rangle}\ , \qquad b_0 = 0\ , \qquad (11)$$

$$|n+1\rangle \equiv \mathcal{H}|n\rangle - a_n|n\rangle - b_n|n-1\rangle\ . \qquad (12)$$

A set of about a hundred coefficients $\{a_n, b_n\}$ are needed to get good convergence of the spectra.

In comparing our results with experimental results we introduce the spectral moments by

$$I_T \equiv \int_{-\infty}^{\infty} I(\omega)d\omega\ , \qquad (13)$$

$$M_1 \equiv \int_{-\infty}^{\infty}\omega I(\omega)d\omega/I_T\ , \qquad (14)$$

$$(M_n)^n \equiv \int_{-\infty}^{\infty} (\omega - M_1)^n I(\omega) d\omega / I_T \ . \tag{15}$$

The spectral moments and total intensity are derived directly from the continued fraction coefficients as

$$I_T = \langle 0|0\rangle \ , \quad M_1 = a_0 - E_0 \ , \tag{16}$$

$$M_2 = \sqrt{b_1} \ , \quad M_3 = \sqrt[3]{(a_1 - a_0)b_1} \ . \tag{17}$$

B. Spectra and moments

The energies of those excited states that are coupled by the Raman interaction appear as poles of $A(z)$ with $\gamma \to 0$. Figure 1 shows the excited state energies in the B_{1g} spectra as a function of J_c/J. In the case of the Heisenberg model ($J_c/J = 0.0$), the state with the strongest Raman intensity has the energy $2.98J$,[16,17,25] and is due to the two-magnon bound state. A simple interpretation of the value of this excited-state energy is as follows. In the Ising limit, the ground state is Néel ordered as in Fig. 2(a). The Raman interaction flips a pair of spins at nearest neighbors so that six bonds with parallel spins at both ends appear as in Fig. 2(b). This excitation costs energy $3J$. It is remarkable that $3J$ is close to $2.98J$ obtained by an exact diagonalization method for the isotropic Heisenberg model, despite large quantum spin fluctuations in the ground state.

Two other excited states appear, which have relatively strong Raman intensity at about $4.5J$ and $5.5J$. They have energies more than $4J$, which is the cutoff energy of two magnons obtained by the classical spin-wave theory. This demonstrates the importance of the quantum spin fluctuations in the ground state and of multimagnon contributions to the understanding of the broad Raman intensity in high-energy region of copper oxides.

The nature of these two excited states may be visualized by going to the Ising limit. Namely, we consider

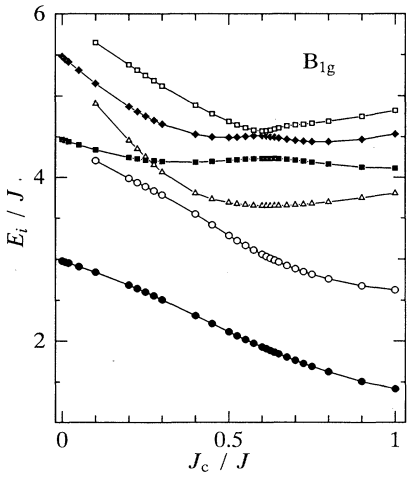

FIG. 1. The J_c/J dependence of excited-state energies E_i. The three states dominating the spectrum are shown by filled marks: the two-magnon bound state (circle), the four-magnon bound state in a plaquette (square), and that in a column (diamond).

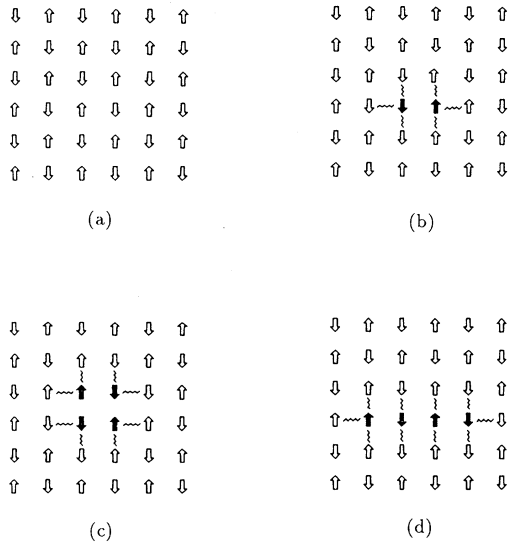

FIG. 2. Spin configurations in the Ising limit. (a) Néel ordered state, (b) two-magnon bound state, (c) four-magnon bound state in a plaquette, and (d) four-magnon bound state in a column.

two pairs of spins flipped in a plaquette or in a column, which are shown in Figs. 2(c) and 2(d). The excitations of these four-magnon bound states cost energies $4J$ and $5J$, respectively. We note that these energies are not much different from the positions of filled squares ($4.5J$) and filled diamonds ($5.5J$) in Fig. 1. Hence, we call these two excited states a four-magnon bound state in a plaquette and one in a column, respectively. Since these flipped configurations extend to the boundary of the 16-site cluster, the finite-size effect plays a more important role than in the two-magnon bound state.

Let us now discuss influences of the four-spin exchange interaction upon the B_{1g} spectra. As shown in Fig. 1 the strongest Raman peak due to the two-magnon bound state is shifted to the lower energy side as J_c/J increases. The dependence of the other excited-state energies on J_c/J is qualitatively similar to that of the two-magnon bound-state energy. However, we notice that the energy of the four-magnon bound state in a plaquette is less sensitive to J_c/J than the energies of other states such as the four-magnon bound state in a column.

In Fig. 3, we present evolution of B_{1g} spectra as we increase the cyclic four-spin exchange starting from the Heisenberg model. We choose a value $\gamma = 0.2J$ to have smooth spectra. In the case of the pure Heisenberg model the intensity of the four-magnon bound state in a plaquette [Fig. 3(c)] with energy about $4.5J$ is less than that of the four-magnon bound state in a column [Fig. 3(d)] with energy about $5.5J$. As J_c/J increases the intensity of the two-magnon bound state [Fig. 3(b)] decreases. Furthermore, at about $J_c/J = 0.25$, the intensity of the four-magnon bound state in a plaquette becomes stronger than that of another four-magnon bound state. This change of relative intensities is an important consequence of the four-spin exchange.

It should also be noted that a new excited state

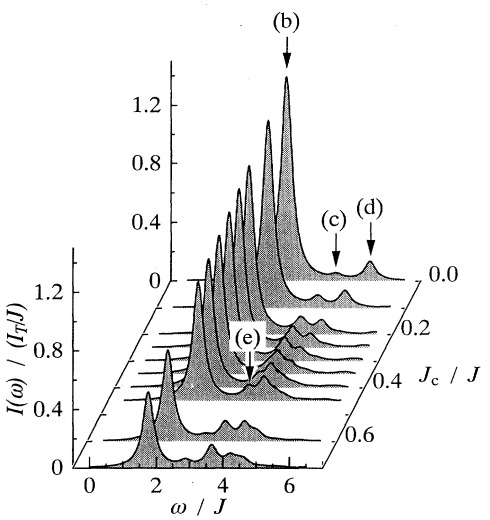

FIG. 3. The evolution of spectra with B_{1g} symmetry with increasing J_c/J. The spectral intensity is normalized by a total intensity obtained from Heisenberg model: (b) two-magnon bound state, (c) four-magnon bound state in a plaquette, (d) four-magnon bound state in a column, and (e) a new excited state. These sublabels correspond to those in Fig. 2 except for (e). We choose $\gamma = 0.2J$.

[Fig. 3(e)] with energy of about $5J$ appears for $J_c/J > 0.1$. The energy of this new excited state as a function of J_c is shown by triangles in Fig. 1. This excited state has a remarkably large Raman intensity, which is comparable to the main peak for $J_c/J > 1.0$ and survives up to the maximum ratio $J_c/J = 1.5$ we have taken.

In the region of the parameter $J_c/J = 0.3$–0.6, both the plaquette and the column four-magnon bound states, and this new excited state have nearly the same energy of about $4J$. Thus in the broadened spectrum they form a conspicuous shoulder in the high-energy side of the main peak. As a result the computed spectral shape with the B_{1g} symmetry becomes similar to the experimental results at 30 K. It should be remarked that this value $J_c/J = 0.3$–0.6 is roughly consistent with the independent theoretical estimate $J_c/J = 0.28$.[19]

In the region with $J_c/J > 0.6$ the spectral line shape is separated into two parts, which stem from the two-magnon bound state and the new excited state, respectively. Thus we conclude that in the large J_c/J region the nature of the spectrum is different from that in the small J_c/J region and the boundary between these two regions corresponds to $J_c/J = 0.3$–0.6.

Let us now turn to quantitative study of spectral moments. M_2 is related to width of the whole spectrum and M_3 to asymmetry of the spectrum. The ratios M_2/M_1 and M_3/M_1 are independent of J, and represent characteristic shape of the Raman spectrum. The ratios have been measured for some materials experimentally. If one takes average over ratios obtained at room temperature for various copper oxides and for a few laser wavelengths, one obtains $M_2/M_1 \sim 0.26$ and $M_3/M_1 \sim 0.21$ for the B_{1g} symmetry.[15] The theoretical values[14] obtained by the Ising-type expansion have been compared favorably with these experimental values. On the other hand, the ratios calculated from the experimental spectra with the high-energy shoulder at $T = 30$ K are larger than those at room temperature. The averaged ratios at low temperature are $M_2/M_1 \sim 0.36$ and $M_3/M_1 \sim 0.31$.[26]

The computed spectral moments are shown in Table I for the present model with $J_c/J = 0.25$. The ratios M_2/M_1 and M_3/M_1 for our model are larger than those for the Heisenberg model. In addition to these ratios we also calculate the ratio between the energy of the two-magnon bound state ω_{2M} and M_1. We obtain 0.88 as a value of ω_{2M}/M_1 with $J_c/J = 0.25$. This value is smaller than that for the Heisenberg model and agrees very well with experimental results. Namely the experimental value of ω_{2M}/M_1 are about 0.88 at room temperature and 0.84 at 30 K. We note again that the experimental ratios are averaged values for some copper oxides and for a few laser wavelengths.

One can extract the value of J from comparison between theory and experiments. Using the calculated values of M_1 we have determined J from experimental data at 30 K for La_2CuO_4 and Nd_2CuO_4. We use the value for M_1 determined by the average for different laser wavelengths. Table II shows J thus extracted. It is evident that J determined with account of the four-spin exchange is larger than that of the Heisenberg model. Since our result is affected by a size effect and special symmetry of the 16-site cluster, we should be careful in discussing the absolute value of J. However, the four-spin exchange should influence the determination of J in the same direction even in the macroscopic size of the system.

We have investigated a spectrum with A_{1g} symmetry as well. Because the Heisenberg Hamiltonian and a Raman interaction for A_{1g} symmetry are commutative, the spectral intensity should be absent in the Heisenberg model. On the other hand our Hamiltonian does not commute with the Raman interaction because of the four-spin exchange. Thus the model gives finite intensity to the A_{1g} spectrum. However, the numerical calculation shows that the ratio of the integrated intensity with the A_{1g} symmetry to that with B_{1g} symmetry is about one to thirty. This is much less than the ratio experimentally observed. Hence, it is unlikely that the cyclic four-spin

TABLE I. Calculated spectral moments with B_{1g} symmetry and their ratios obtained by the exact diagonalization method; ω_{2M} is the energy of the two-magnon bound state making the main peak. M_2/M_1 and M_3/M_1 depend only on J/J_c.

	J_c/J	ω_{2M}	M_1	M_2	M_3	M_2/M_1	M_3/M_1	ω_{2M}/M_1
Heisenberg model	0.00	$2.98J$	$3.24J$	$0.80J$	$1.14J$	0.25	0.35	0.92
This study	0.25	$2.60J$	$2.97J$	$0.84J$	$1.11J$	0.28	0.37	0.88

TABLE II. Theoretical estimates of J with and without account of the four-spin exchange.

	Sample	J (cm^{-1})
$J_c/J = 0.0$	La_2CuO_4	1200
	Nd_2CuO_4	1060
$J_c/J = 1/4$	La_2CuO_4	1300
	Nd_2CuO_4	1160

exchange interaction is responsible for the large A_{1g} intensity in actual CuO_2 planes. This result suggests the presence of another Raman interaction. For example, the small charge-transfer energy in CuO_2 planes may induce a considerable size of the Raman interaction, which flips a pair of next-nearest-neighbor spins.

IV. EFFECTS OF FOUR-SPIN INTERACTION ON THE GROUND STATE

A. Ground-state energy and symmetry

We varied cyclic four-spin exchange interaction J_c/J from zero (pure Heisenberg model) up to 1.5. Figure 4 shows the J_c/J dependence of the ground-state energy and a low-lying energy, which has the Γ_2 (B_{1g}) symmetry in the 16-site cluster. The ground-state energy becomes maximum at $J_c/J \sim 0.6$. In the whole parameter region the ground state has the Γ_1 (A_{1g}) symmetry and there is no change in the ground-state symmetry. On the contrary, for 10- and 18-spin systems the change of the symmetry does happen in the ground states. Thus the symmetry depends on a way to take spin clusters. However, the J_c/J dependence of the energies are similar to the case of the 16-site cluster. In subsequent discussions on effects of the cyclic four-spin exchange, we concentrate on 16-site spin system.

B. Staggered magnetization

In the finite size of the cluster there is no long-range order such as the Néel order, but Néel-like correlations are present. In order to see the degree of Néel-like correlations we take the following quantity:

$$m_s = \frac{1}{N}\sqrt{3\left\langle \Psi_0 \left| \left(\sum_i \varepsilon_i S_i^z \right)^2 \right| \Psi_0 \right\rangle}\ , \tag{18}$$

where ε_i is $+1$ or -1, depending on whether i is on the A or B sublattice.[27] In the complete Néel state one has $m_s = \sqrt{3/4} \sim 0.87$, and m_s decreases as the wave function $|\Psi_0\rangle$ loses the Néel-like correlation. Thus it is appropriate to call m_s the staggered magnetization. It is necessary to discuss the size dependence[27] in order to evaluate absolute value of m_s for the macroscopic system. However, we restrict ourselves to the 16-site cluster here and discuss qualitative modification of staggered magnetization caused by the cyclic four-spin exchange.

Figure 5 shows the dependence of staggered magnetization on J_c/J. With increase of J_c/J from zero m_s increases rapidly up to about 0.78 at a critical value of $J_c/J = 0.8$ and then decreases with further increase of J_c/J. The maximum value $m_s \sim 0.8$ is close to that of the Néel state and is considerably larger than that of the Heisenberg model ($m_s \sim 0.52$) with the same size of the cluster. We note that the value $J_c/J = 0.8$, which gives maximum m_s is larger than the one $J_c/J = 0.6$, which gives the maximum ground-state energy.

C. Contributions of each interaction to total energy

From Eqs. (1) and (2), we rewrite $\mathcal{H}$ as follows:

$$\mathcal{H} = \mathcal{H}_1 + \mathcal{H}_2 + \mathcal{H}_P + \mathcal{H}_D\ , \tag{19}$$

$$\mathcal{H}_1 = \left(J - \frac{J_c}{2}\right) \sum_{\langle i,j \rangle} \mathbf{S}_i \cdot \mathbf{S}_j\ , \tag{20}$$

$$\mathcal{H}_2 = -\frac{J_c}{4} \sum_{\langle j,j' \rangle} \mathbf{S}_j \cdot \mathbf{S}_{j'}\ , \tag{21}$$

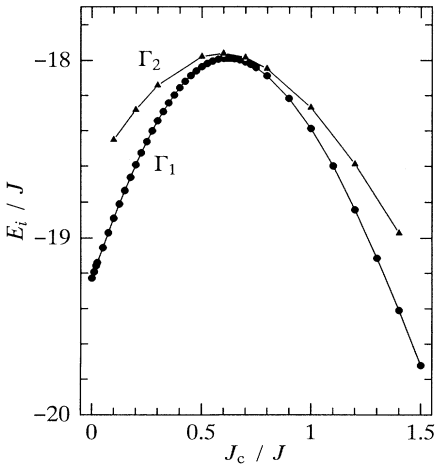

FIG. 4. The J_c/J dependence of the ground-state energy and the lowest energy of states with the Γ_2 symmetry. The ground state has the Γ_1 symmetry in the whole parameter region and there is no crossover of energies in the case of the 4×4 square lattice.

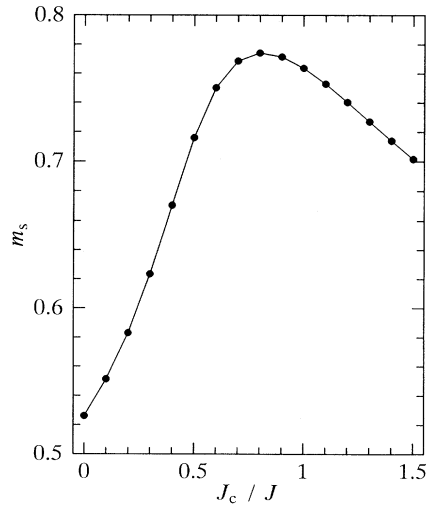

FIG. 5. The staggered magnetization m_s as a function of J_c/J.

$$\mathcal{H}_P = \frac{J_c}{4} \sum_{\langle i,j,k,l \rangle} (P_{ijkl} + P_{ijkl}^{-1}) \ , \tag{22}$$

$$\mathcal{H}_D = -\frac{J}{4} \sum_{\langle i,j \rangle} n_i n_j - \frac{J_c}{16} N \ , \tag{23}$$

where $\mathcal{H}_1$ and $\mathcal{H}_2$ represent nearest-neighbor and next-nearest-neighbor spin exchanges, respectively. $\mathcal{H}_P$ gives cyclic four-spin permutations in the smallest plaquette. The diagonal part $\mathcal{H}_D$, which do not influence spin configurations will not be considered hereafter. We define $\mathcal{H}_S \equiv \mathcal{H}_1 + \mathcal{H}_2 + \mathcal{H}_P$ as the sum of three types of exchange interactions.

We now discuss dependence of $\langle \mathcal{H}_S \rangle$ on J_c/J and contributions of each spin exchange Hamiltonian. Here $\langle \cdots \rangle$ means expectation value with respect to the ground state. Figure 6 shows the result of calculation. It is found that the value of J_c/J, which gives the maximum of $\langle \mathcal{H}_S \rangle$ agrees with the value of J_c/J for the staggered magnetization. This value of J_c/J is remarkably close to a point where the contribution of the four-spin permutation to $\langle \mathcal{H}_S \rangle$ becomes larger than that of the next-nearest-neighbor exchange. For instance in the 16-site system, $\langle \mathcal{H}_P \rangle$ dominates over $\langle \mathcal{H}_2 \rangle$ beyond about $J_c/J \sim 0.9$. This result suggests that there are two regions of J_c/J, each of which gives the ground-state spin configuration with nature fundamentally different from each other.

D. Wave function of ground state

In the presence of quantum spin fluctuations, many spin configurations contribute to the wave function $|\Psi_0\rangle$ of the ground state:

$$|\Psi_0\rangle = \sum_{\alpha} c_\alpha |\alpha\rangle \ , \tag{24}$$

where $|\alpha\rangle$ denotes a spin configuration basis. The coefficient c_α is in general complex. Actually the coefficients numerically derived turn out to be real in the parameter range we have studied, as in the case of the Heisenberg model.[28] To be specific we discuss the spin structure of the 16-site ground state. In contrast to a one-body wave function, it is not straightforward to visualize the many-body wave function. Hence we need a quantity that represents the character of the wave function in a comprehensible manner.

Let us introduce for this purpose a quantity δ_α, which represents the deviation of a spin configuration basis $|\alpha\rangle$ from the Néel basis. Namely, δ_α is defined by

$$\delta_\alpha = \left\langle \alpha \left| \sum_{\langle i,j \rangle} S_i^z S_j^z \right| \alpha \right\rangle - \left\langle \text{Néel} \left| \sum_{\langle i,j \rangle} S_i^z S_j^z \right| \text{Néel} \right\rangle \ , \tag{25}$$

where $|\text{Néel}\rangle$ is one of the two bases with the Néel spin configuration. The whole set of spin configuration bases is classified in terms of the deviation δ_α. Then with use of δ_α a ground state is characterized by a distribution of weight $W(\delta)$, which is defined by

$$W(\delta) \equiv \sum_{\alpha \in \{\delta_\alpha = \delta\}} c_\alpha^2 \ , \tag{26}$$

where $\sum_{\alpha \in \{\delta_\alpha = \delta\}}$ means a sum over such spin configurations that have the specified deviation δ.

The results of $W(\delta)$ are shown in Fig. 7 for some values of J_c/J. We notice that $J_c/J = 0.8$ corresponds to the maximum staggered magnetization m_s. In the case of the Heisenberg model ($J_c/J = 0$), all spin configurations with δ less than eight have weights comparable to that of the Néel spin configuration. However, the weight of a spin configuration with $\delta = 4$ is small relative to the others. This is, in fact, a common character of the ground state in the region where J_c/J is smaller than 0.8. With inclusion of the cyclic four-spin exchange, the weight of Néel configuration increases up to the maximum of about 70% at $J_c/J = 0.8$. On the other hand, the weight of spin configurations with large δ decreases.

We interpret the reason for the growth of the Néel configuration as follows: Since J_c is positive, the next-

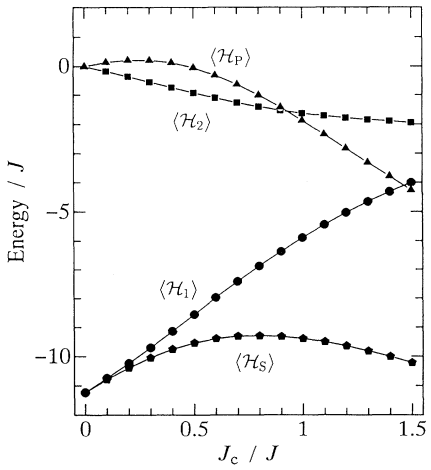

FIG. 6. Contribution of various parts of the exchange Hamiltonian to the ground-state energy as a function of J_c/J.

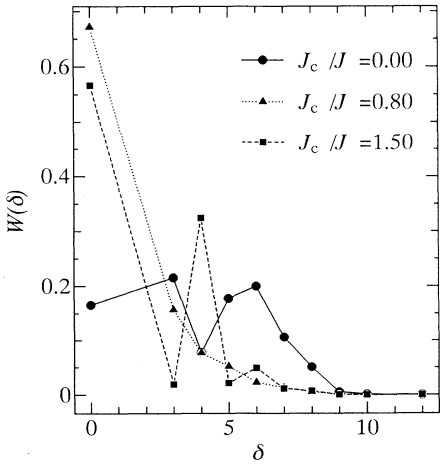

FIG. 7. The distribution of weight $W(\delta)$ in the ground state as a function of δ which is defined in the text.

nearest-neighbor exchange part $\mathcal{H}_2$ does not frustrate the antiferromagnetic order caused by the nearest-neighbor exchange $\mathcal{H}_1$. Therefore the Néel-spin configuration is favorable for both types of exchanges. Within the region where the four-spin permutation Hamiltonian $\mathcal{H}_P$ does not contribute so much, the exchange Hamiltonians $\mathcal{H}_1$ and $\mathcal{H}_2$ dominate the total energy. Thus the Néel configuration is enhanced in the ground state. At $J_c/J = 0.8$ the structure of the ground state is closest to the Néel order.

As J_c/J increases beyond the critical value 0.8, another structure grows. In this region of J_c/J the spin configurations with $\delta = 4$ plays an important role. The structure of the ground state mainly consists of Néel-spin configurations and one of the configurations with $\delta = 4$ in contrast with the region $J_c/J < 0.8$. The weight of $\delta = 4$ comes mainly from such spin configuration that involves neighboring four spins in a plaquette flipped relative to the Néel background [Fig. 2(c)]. In the case of $J_c/J = 1.5$, the relative weight of this particular configuration amounts to about 85% of such spin configurations with $\delta = 4$. This result is consistent with the fact that the four-spin permutation part of the full Hamiltonian contributes to the total energy more than the next-nearest-neighbor spin exchange in the region of $J_c/J > 0.8$. Thus the critical value $J_c/J = 0.8$, which gives the maximum staggered magnetization, divides the two regions of ground states, each of which has a different nature of spin structures.

E. Spin-spin correlations

The spin-spin correlation function $\langle S_0^z S_R^z \rangle$ at equal times has been widely used as a convenient quantity showing the character of the magnetic system. We present results of the spin-spin correlation in Fig. 8. Let us first note a particular situation in the Heisenberg model on the 4×4 square lattice with the periodic boundary condition. Namely, the spin-spin correlation at distance $R = \sqrt{2}$ is equivalent to that at $R = 2$. Here a pair of spins separated by one of these distances are coupled with each other via two spins, which belong to another sublattice. Hence, the spin-spin correlations corresponding to $R = \sqrt{2}$ and 2 have exactly the same value in the Heisenberg model with only the nearest-neighbor exchange.

Below the critical value $J_c/J = 0.8$ corresponding to the maximum staggered magnetization, the cyclic four-spin exchange enhances spin-spin correlations at all distances. The difference between spin-spin correlations of $R = \sqrt{2}$ and 2 remain small in this parameter region, though the distances are no longer equivalent with finite J_c. At the critical value $J_c/J \sim 0.8$ the spin-spin correlation function takes the values closest to the Néel state.

Above the critical point, on the other hand, the Néel-like spin correlations are disturbed by the plaquette spin configurations in the ground state. In this parameter region we have found a large difference between the value of spin-spin correlations with $R = \sqrt{2}$ and that with $R = 2$ (Fig. 9). Namely, the spin-spin correlation with $R = 2$ is more strongly disturbed than that with $R = \sqrt{2}$. An intuitive explanation for this difference is as follows. Let us choose a spin in the plaquette with flipped spins relative to the Néel background [Fig. 2(c)]. This spin has four next-nearest-neighbor spins separated by $R = \sqrt{2}$, and four third-nearest-neighbor spins separated by $R = 2$. In the presence of the complete Néel order, all these spins should be parallel to each other because a pair of spins separated by these distances belong to the same sublattice. In the plaquette spin configuration, however, all third-nearest-neighbor spins become antiparallel to the chosen spin. On the contrary, one of the four next-nearest-neighbor spins is inside the plaquette and is parallel to the chosen spin. Therefore, the spin-spin correlation with $R = \sqrt{2}$ survives the disturbance caused by the four-spin exchange more stubbornly than the correlation with $R = 2$.

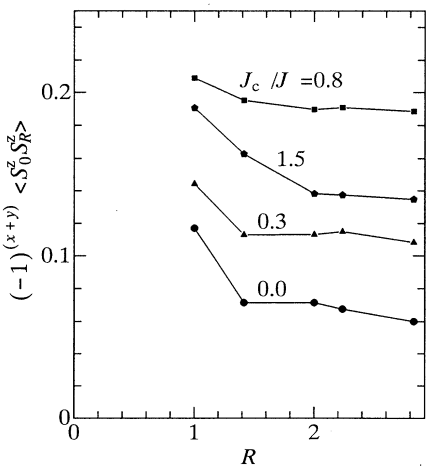

FIG. 8. The spin-spin correlation times the phase factor $(-1)^{x+y}\langle S_0^z S_R^z \rangle$ as a function of $R(= \sqrt{x^2+y^2})$ for representative values of J_c/J. The phase factor is -1 if R belongs to the sublattice different from that of the site 0.

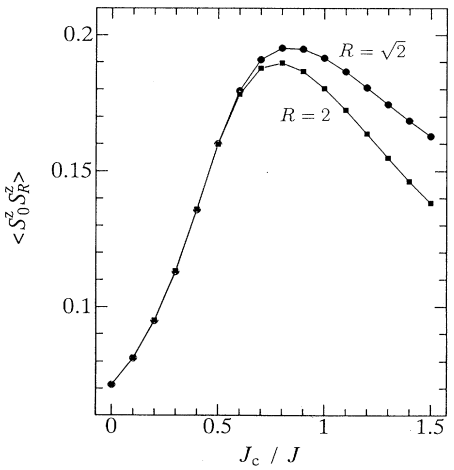

FIG. 9. The dependence of $\langle S_0^z S_R^z \rangle$ on J_c/J for $R = 2$ and $R = \sqrt{2}$.

V. CONCLUSIONS

We have investigated the influences of the cyclic four-spin exchange interaction J_c upon the magnetic Raman-scattering spectra and properties of the ground states with the use of the exact diagonalization method for small clusters. Let us summarize the main results of the present study. First, it is found that the cyclic four-spin exchange reduces the energy of the two-magnon bound state. The analysis of Raman-scattering data in the light of this new information leads to a larger Heisenberg exchange interaction J than that obtained with use of the pure Heisenberg model.

Secondly the cyclic four-spin exchange enhances scattering intensities of some multimagnon states with the energy of about $4J$ in the realistic case of $J_c/J = 0.3$. We thus suggest a correspondence between this new scattering feature and the shoulder observed in the experimental spectra at 30 K.[6] In the hypothetical region, where J_c is larger than J, the Raman spectra have simple structures consisting of two peaks only.

Thirdly we have derived the ratios of spectral moments M_2/M_1 and M_3/M_1, which are larger than those in the Heisenberg model. We have also calculated the ratio ω_{2M}/M_1 and have found better agreement with experimental results both at room temperature and at 30 K.

Though our investigations are for a finite-sized cluster, our results by an exact diagonalization method should provide a qualitative information about the effect of J_c in macroscopic systems. Since the realistic value of J_c is comparable with the thermal energy of low temperature, the effects of the cyclic four-spin exchange interaction may be significant only for experiments at low temperatures. Actually the shoulders in the B_{1g} spectra are observed only in the experiments at 30 K. We suggest that the peak around $4J$, which grows with inclusion of J_c is closely related to the high-energy shoulder of experimental spectra.

Finally we have shown that the four-spin exchange leads to two kinds of ground states depending on the ratio J_c/J. In the boundary that corresponds to $J_c/J \sim 0.8$, the Néel configuration dominates the ground state. For larger J_c/J, plaquette spin configurations also play an important role. Our investigations in the present paper have been limited to the insulating phase. It is a very interesting subject to examine the role of J_c in the metallic phase of high-T_c copper oxides.

ACKNOWLEDGMENT

We would like to thank Dr. S. Sugai for providing us with experimental data of spectral moments.

[1] K. B. Lyons, P. A. Fleury, J. P. Remeika, A. S. Cooper, and T. J. Negran, Phys. Rev. B **37**, 2353 (1988).
[2] K. B. Lyons, P. A. Fleury, L. F. Schneemeyer, and J. V. Waszczak, Phys. Rev. Lett. **60**, 732 (1988).
[3] S. Sugai, S. Shamoto, and M. Sato, Phys. Rev. B **38**, 6436 (1988).
[4] K. B. Lyons and P. A. Fleury, J. Appl. Phys. **64**, 6075 (1988).
[5] K. B. Lyons, P. E. Sulewski, P. A. Fleury, H. L. Carter, A. S. Cooper, G. P. Espinosa, Z. Fisk, and S-W. Cheong, Phys. Rev. B **39**, 9693 (1989).
[6] S. Sugai, M. Sato, T. Kobayashi, J. Akimitsu, T. Ito, H. Takagi, S. Uchida, S. Hosoya, T. Kajitani, and T. Fukuda, Phys. Rev. B **42**, 1045 (1990).
[7] G. Shirane, Y. Endoh, R. J. Birgeneau, M. A. Kastner, Y. Hidaka, M. Oda, M. Suzuki, and T. Murakami, Phys. Rev. Lett. **59**, 1613 (1987).
[8] T. Thio, T. R. Thurston, N. W. Preyer, P. J. Picone, M. A. Kastner, H. P. Jenssen, D. R. Gabbe, C. Y. Chen, R. J. Birgeneau, and A. Aharony, Phys. Rev. B **38**, 905 (1988).
[9] R. J. Birgeneau, D. R. Gabbe, H. P. Jenssen, M. A. Kastner, P. J. Picon, and T. R. Thurston, Phys. Rev. B **38**, 6614 (1988).
[10] G. Aeppli, S. M. Hayden, H. A. Mook, Z. Fisk, S-W. Cheong, D. Rytz, J. P. Remeika, G. P. Espinosa, and A. S. Cooper, Phys. Rev. Lett. **62**, 2052 (1989).
[11] P. A. Fleury and H. J. Guggenheim, Phys. Rev. Lett. **24**, 1346 (1970).
[12] R. J. Elliott and M. F. Thorpe, J. Phys. C **2**, 1630 (1969).
[13] J. B. Parkinson, J. Phys. C **2**, 2012 (1969).
[14] R. R. P. Singh, P. A. Fleury, K. B. Lyons, and P. E. Sulewski, Phys. Rev. Lett. **62**, 2736 (1989).
[15] P. E. Sulewski, P. A. Fleury, K. B. Lyons, S-W. Cheong, and Z. Fisk, Phys. Rev. B **41**, 225 (1990).
[16] E. Dagotto and D. Poilblanc, Phys. Rev. B **42**, 7940 (1990).
[17] E. Gagliano and S. Bacci, Phys. Rev. B **42**, 8772 (1990).
[18] M. S. Hybertsen, E. B. Stechel, M. Schüter, and D. R. Jennison, Phys. Rev. B **42**, 11068 (1990).
[19] H. J. Schmidt and Y. Kuramoto, Physica C **167**, 263 (1990).
[20] Y. Honda, Y. Kuramoto, and T. Watanabe, Physica C **185-189**, 1493 (1991).
[21] M. Roger, J. H. Hetherington, and J. M. Delrieu, Rev. Mod. Phys. **55**, 1 (1983).
[22] P. A. Fleury and R. Loudon, Phys. Rev. **166**, 514 (1968).
[23] E. R. Gagliano, E. Dagotto, A. Moreo, and F. C. Alcaraz, Phys. Rev. B **34**, 1677 (1986).
[24] E. R. Gagliano and C. A. Balseiro, Phys. Rev. Lett. **59**, 2999 (1987).
[25] M. Roger and J. M. Delrieu, Phys. Rev. B **39**, 2299 (1989).
[26] S. Sugai (private communication).
[27] J. D. Reger and A. P. Young, Phys. Rev. B **37**, 5978 (1988).
[28] W. Marshall, Proc. R. Soc. London, Ser. A **232**, 48 (1955).